Polarization of light from warm clouds above an accretion disk: effects of strong-gravity near a black hole

Jiří Horák and Vladimír Karas

Astronomical Institute, Academy of Sciences, Boční II, CZ-141 31 Prague, Czech Republic

Abstract

We study polarization from scattering of light on a cloud in radial motion along the symmetry axis of an accretion disk. Radiation drag from the disk and gravitational attraction of the central black hole are taken into account, as well as the effect of the cloud cooling in the radiation field. This provides us with a self-consistent toy-model for predicted lightcurves, including the linear polarization that arises from the scattering. Strong gravitational lensing creates indirect images; these are formed by photons that originate from the disk, get backscattered onto the photon circular orbit and eventually redirected towards an observer. Under suitable geometrical conditions the indirect photons may visibly influence the resulting magnitude of polarization and light-curve profiles. Relevant targets are black holes in active galactic nuclei and stellar-mass Galactic black-holes exhibiting episodic accretion/ejection events.

Key words: relativity — polarization – accretion disks — black holes — scattering — gravitational lensing — accretion, accretion disks

1. Introduction

The present-day evidence for black holes relies almost entirely on information carried by electromagnetic waves. X-rays play a particular role (Seward & Charles 1995): they are supposed to emerge from gas near a black hole horizon and bring us imprints of physical processes and conditions in the place of their origin and along the ray path. Various spectral and lightcurve patterns have been identified as likely signatures of supermassive black holes in galactic nuclei and stellar-mass black holes. These features presumably arise when matter is accreted from an immediate vicinity of the black hole. The ultimate goal of this effort is to prove the existence of event horizons in 'real' nature and this way to discover black holes. Clearly, an affirmative proof is a great challenge that may still be far ahead of us. Here we study a related task, which appears to be somewhat easier on the technical side, though it also represents an unresolved issue as yet: searching for rays of photons that encircle an ultra-compact star or a black hole.

Accretion disks represent a common way of feeding black holes and generating photons, which then experience strong-gravity while travelling to a distant observer (Kato et al. 1998; Krolik 1999). Outside the disk plane density is much less, however, even regions near axis are not empty: winds and jets emerge, roughly along the symmetry axis. We address a question whether future observations of polarized time-dependent signal can help recognizing the effects of strong-gravity light bending, and what features are expected in light curves. To this aim we examine a model of warm clouds moving radially along the symmetry axis. Primary photons from the disk are Thomson-scattered and polarized. We assume that the process takes place near a Schwarzschild black hole, where the higher-order (indirect) light rays contribute to the observed radiation flux. The resulting modulation of intensity and polarization magnitude can reach a non-negligible level under suitable geometrical alignment of the black hole, the cloud and the observer. We treat the interaction of the cloud with the radiation and gravitational fields in the relativistic framework (Abramowicz et al. 1990; Vokrouhlický & Karas 1991; Keane et al. 2001). This approach provides us with a self-consistent description of the cloud motion and the resulting observed signal. Both ingredients are conveniently expressed in terms of the radiation stress tensor.

There is the evidence for jets being formed only a few tens gravitational radii from a supermassive central black hole (Junor et al. 1999). The emission mechanisms producing the observed high-energy photons (X- and γ-rays) are likely non-thermal, but it is not clear whether the synchrotron emission or the inverse Compton emission dominates in each particular source (Harris & Krawczynski 2002). Here we concentrate on the latter case (within the Thomson approximation), which seems to be relevant for radio-quiet sources with the ambient radiation acting on particles and fluids and determining their terminal (equilibrium) speed; see Noerdlinger 1974; O'Dell 1981; Sikora & Wilson 1981; and Phinney 1982 for original papers. This dynamical influence of the radiation field has been studied further by Sikora et al. (1996), Renaud & Henri (1998), Tajima & Fukue (1998), Fukue (1999) and Watarai & Fukue (1999). Ghisellini et al. (2004) proposed a model of aborted (failed) jets in which colliding clouds and shells occur very near a black hole and are embedded in strong radiation. According to their scheme, most of energy dissipation should take place on the symmetry axis of an accretion disc where the individual clouds either move away from the black hole, or they fall back. The process of gravitational and radiative

acceleration of plasma was studied also by Fukue et al. (2001) and Fukue (2005), who examined the efficiency of collimation towards the disk axis and applied this model to the case of microquasars.

The effects of strong gravity are significant in this region and the challenge for future techniques is to identify subtle, yet specific patterns in X-ray lightcurves. Polarization studies could help to achieve this goal. Distinct features should arise from multiple trajectories of light rays connecting the source with the observer along several different paths. The rays winding up around the photon circular orbit should experience a characteristic mutual time delay. We discuss the expected features in this paper.

Polarization of light from scattering in winds and jets was examined by various authors. Following the early papers (e.g. Dolan 1967; Angel 1969; Bonometto et al. 1970), Begelman & Sikora (1987) studied the linear polarization of initially unpolarized soft radiation up-scattered by cold electrons in a jet. Beloborodov (1998) examined the case of fast winds outflowing from an accretion disk slab. He found that polarization direction depends on the wind velocity; the terminal speed of the outflow plays a critical role. Poutanen (1994) and Celotti & Matt (1994) considered the synchrotron self-Compton mechanism, a likely process producing polarization wherever magnetic fields interact with relativistic particles. The effect of electron temperature was also discussed: it reduces the final magnitude of polarization. Recently, Lazzatti et al. (2004) further discussed the Compton drag as a conceivable mechanism for polarization in gamma-ray bursts. Horák & Karas (2005) studied the polarization of scattered light from a compact star, taking into account the light-bending effect. In fact, it was demonstrated that retro-lensing images, which clearly require strong gravity, can give rise to specific polarimetric signatures in predicted lightcurves. Here we develop this model further by considering nonnegligible temperature of the scattering medium and by changing the geometry of the primary source. We assume a Keplerian disk as the source, so we are able to examine situations that are relevant for accreting black holes.

2. The model setup

As a toy-model for non-uniform outflows and aborted jets we consider a cloud of particles moves through the radiation field of a standard thin accretion disc (Shakura & Sunyaev 1973). The disk defines the equatorial plane $\theta = \pi/2$ of the system. Primary photons from the disc are scattered by electrons in the cloud, they are beamed (preferentially in the direction of the scatterer motion), and polarized by Thomson mechanism. We adopt the first scattering approximation (small optical depth $\tau \ll 1$ of the cloud is assumed) and we restrict the cloud motion to the axis of symmetry, $z \equiv z(t)$. The basic setup of the model is captured in figure 1.

The spacetime metric is (Misner et al. 1973)

$$ds^2 = -\xi dt^2 + \xi^{-1} dr^2 + r^2 \left(d\theta^2 + \sin^2\theta d\phi^2 \right), \qquad (1)$$

where $\{t, r, \theta, \phi\}$ are Schwarzschild coordinates, $\xi(r) \equiv 1-$
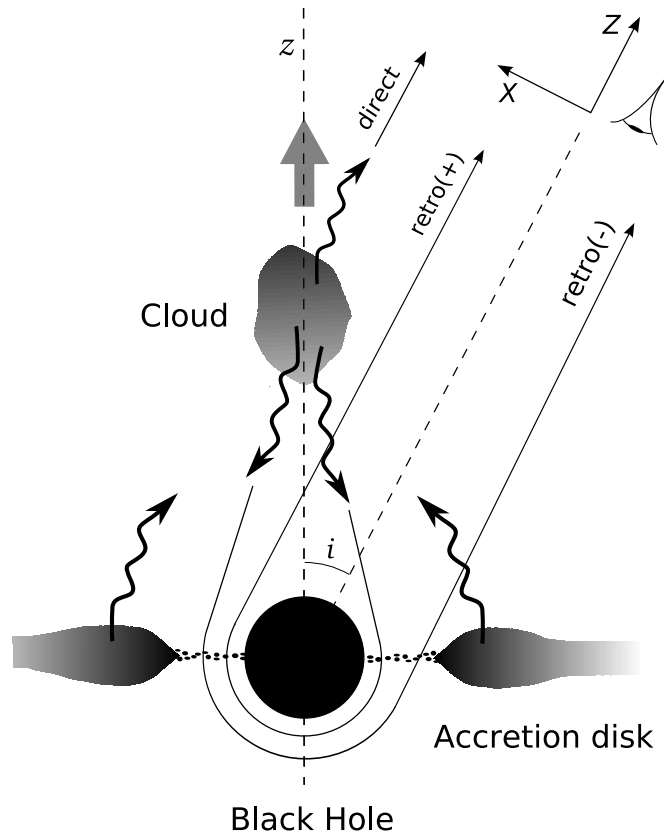
Fig. 1. Geometry of the model. An accretion disk is the source of primary unpolarized light, which is then Thomson scattered on a cloud. The cloud moves radially along the axis, $z \equiv z(t)$, in the radiation field of the disk. Gravity of the central black hole influences the motion of the cloud. The light rays of primary and scattered photons are also affected. Direct and indirect (retro-lensed) light rays have different degree of linear polarization and they experience different amplification and the Doppler boosting. The observed lightcurve is produced by all the rays reaching an observer at view angle i far from the centre (along Z-direction). The indirect photons contribute most significantly to the the total signal if the cloud moves toward the black hole and the observer inclination is small.

$R_{\rm S}/r$ is the redshift function, $R_{\rm S} \equiv 2GM/c^2$. Geometrized units $c = G = 1$ will be used.

The total bolometric luminosity of a standard disk, $L = GM\dot{M}/2R_{\rm in}$, can be scaled by the Eddington luminosity $L_{\rm E} = 4\pi cGMm_{\rm p}/\sigma_{\rm T}$. We thus define $\Lambda \equiv L/L_{\rm E}$. The corresponding intensity emitted from the disk is

$$I_{\rm d}(r) = \frac{m_{\rm p}c^3}{\sigma_{\rm T}R_{\rm S}} \Lambda I_{\rm d\star}, \quad I_{\rm d\star} \equiv \frac{3R_{\rm S}^2 R_{\rm in}}{2\pi r^3} \left(1 - \sqrt{\frac{R_{\rm in}}{r}} \right), (2)$$

where we denoted, by an asterisk, the intensity rescaled to the dimension-less form. Hereafter the radiation terms will be made dimension-less by scaling them with $(m_{\rm p}c^3/\sigma_{\rm T}R_{\rm S})\Lambda$.

Photons travel along null geodesics and give rise to the radiation stress tensor at every point outside the disk plane and above the black hole horizon. Figure 2 shows the dependence of the components relevant for our cal-
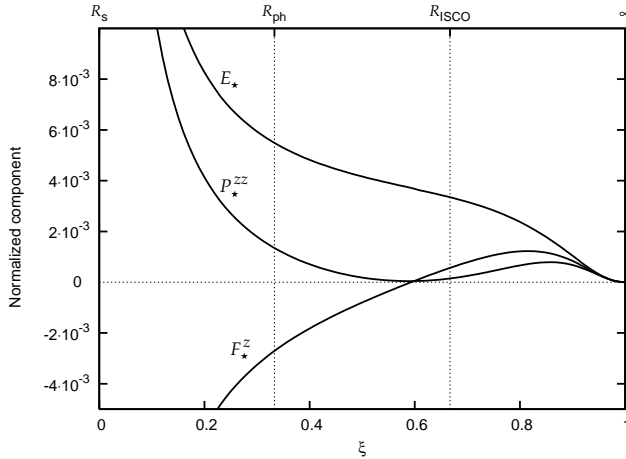
Fig. 2. Normalized components of the radiation stress tensor on the symmetry axis for radiation originating from a standard disk. The inner edge of the disk corresponds to the innermost stable circular orbit, $R_{\rm in} = R_{\rm ISCO} = 3R_{\rm S}$; no intervening matter is considered below that radius. The outer edge is at $R_{\rm out} = 10^3 R_{\rm S}$. Location of the photon circular orbit $R_{\rm ph} = 1.5 R_{\rm S}$ is also indicated.

culation on symmetry axis of the black hole – accretion disk system (we employ similar notation for the radiation stress tensor components as e.g. Fukue & Hachiya 1999; Watarai & Fukue 1999).

In spite of the fact that we employ a particular model of a thin accretion disk in this paper, several rather general features are captured in Fig. 2 that we expect to shape the radiation field of astrophysically realistic models too. These can be summarized as follows.

- The radiation stress tensor vanishes for $z \to \infty$ ($\xi \to 1$) because the angular size of the disk, as observed by distant observers, decreases to zero.
- Far from the centre, tz-component of the stress tensor (measured by a static observer) is positive, however, this term changes its sign at certain value of height z near above the disk. This effect operates for a static observer inside photon circular orbit, who intercepts photons falling into the black hole.
- All three components diverge as $z \to R_{\rm S}$ ($\xi \to 0$). Close to the horizon the accretion disk appears again as a point-like source producing the energy density $\propto \xi^{-1}(z)$. Here, two effects act against each other: the gravitational bending of light-rays reduces the solid angle that the disk occupies on the observer local sky by factor $\propto \xi$, whereas the gravitational redshift increases the radiation intensity by factor $\propto \xi^{-2}$ (blueshift occurs, in fact).

Intensity of scattered light and its polarization are characterized by Stokes parameters (Chandrasekhar 1960; Rybicky & Lightman 1979). These can be obtained by integrating over all directions $\boldsymbol{n}_i$ of photons incident on scattering particles of the cloud from different points in the disk (Horák & Karas 2005):

$$\bar{I} = \bar{E} + \bar{P}^{ZZ}, \tag{3}$$

$$\bar{Q} = \bar{P}^{YY} - \bar{P}^{XX}, \tag{4}$$

$$\bar{U} = -2\bar{P}^{XY}, \tag{5}$$

where bars denote quantities in the comoving orthonormal polarization frame, $\bar{X}$-axis of which is given by projecting the symmetry axis onto the observing plane and $\bar{Z}$-axis coinciding with the direction of scattered photons. $\bar{P}^{AB}$ are local components of the radiation stress tensor (the spatial part of the energy-momentum tensor $\bar{T}^{(\alpha)(\beta)}$, $\bar{E} \equiv \bar{T}^{(t)(t)}$ is local energy-density. The values of Stokes parameters (3)–(4) are normalized by $A \equiv 3\tau/16\pi$, $\tau \equiv n_{\rm e}\sigma_{\rm T}R$ is the Thomson optical depth of the cloud in terms of electron density $n_{\rm e}$, $R \ll R_{\rm S}$ is radius of the cloud. Polarization is purely linear ($V=0$) and its the magnitude is equal to $\Pi = (\bar{Q}^2 + \bar{U}^2)^{1/2}/\bar{I}$.

3. Polarization from scattering on warm clouds near a black hole

So far we assumed the cloud to be cold and we did not consider any microscopic (random) motion of the scattering electrons within the cloud volume. Hereafter, in order to account for the electron temperature we average the equations (3)–(5) over the electron distribution $n(\boldsymbol{\beta}_{\rm e}) = n_{\rm e} f(\gamma_{\rm e})$ in the cloud comoving frame (CCF), where the electron distribution is entirely isotropic and $\gamma_{\rm e} \equiv (1 - \beta_{\rm e}^2)^{-1/2}$ is the corresponding Lorentz factor. Stokes parameters are first evaluated in the local electron comoving frame (ECF), Lorentz transformed to the CCF, and the result is averaged over random velocities of the electrons. We obtain

$$\bar{I} = (1+\mathcal{A})\left(\bar{E} + \bar{P}^{ZZ}\right) + \mathcal{B}\left(\bar{E} - 3\bar{P}^{ZZ}\right) - 2\mathcal{A}\bar{F}^Z, \tag{6}$$

$$\bar{Q} = \bar{P}^{YY} - \bar{P}^{XX}, \tag{7}$$

$$\bar{U} = -2\bar{P}^{XY}, \tag{8}$$

where F^Z is the radiation flux component measured in direction of the photon after scattering. We introduced mean values

$$\mathcal{A} \equiv \frac{4}{3}\left\langle \gamma_{\rm e}^2 \beta_{\rm e}^2 \right\rangle, \quad \mathcal{B} \equiv 1 - \left\langle \frac{\ln[\gamma_{\rm e}(1+\beta_{\rm e})]}{\beta_{\rm e}\gamma_{\rm e}^2} \right\rangle; \tag{9}$$

$\langle x \rangle \equiv \int x f(\gamma_{\rm e}) \, \mathrm{d}\gamma_{\rm e}$ denotes averaging over the electron energy distribution; see Horák (2005) for details of the derivation of eqs. (6)–(8).

The Lorentz boost from CCF to the static frame introduces the familiar factor $\mathcal{D}^4$, where $\mathcal{D} = \gamma^{-1}(1-\beta\cos\vartheta)^{-1}$ is the Doppler factor, $\gamma = (1-\beta^2)^{-1/2}$, β is the cloud bulk velocity and ϑ is the angle between this velocity and the scattered photon direction:

$$I = \mathcal{D}^4\bar{I}, \quad Q = \mathcal{D}^4\bar{Q}, \quad U = \mathcal{D}^4\bar{U}. \tag{10}$$

In this way the frequency-integrated Stokes parameters are found in terms of the radiation stress tensor components. The relation between the CCF components $(\bar{E}, \bar{F}^A, \bar{P}^{AB})$ and the static frame components (E, F^a, P^{ab}) is

$$\bar{P}^{XX} = \mathcal{D}^2\left[P^{xx}(\cos\vartheta - \beta)^2 + \gamma^2\Delta\sin^2\vartheta\right], \tag{11}$$
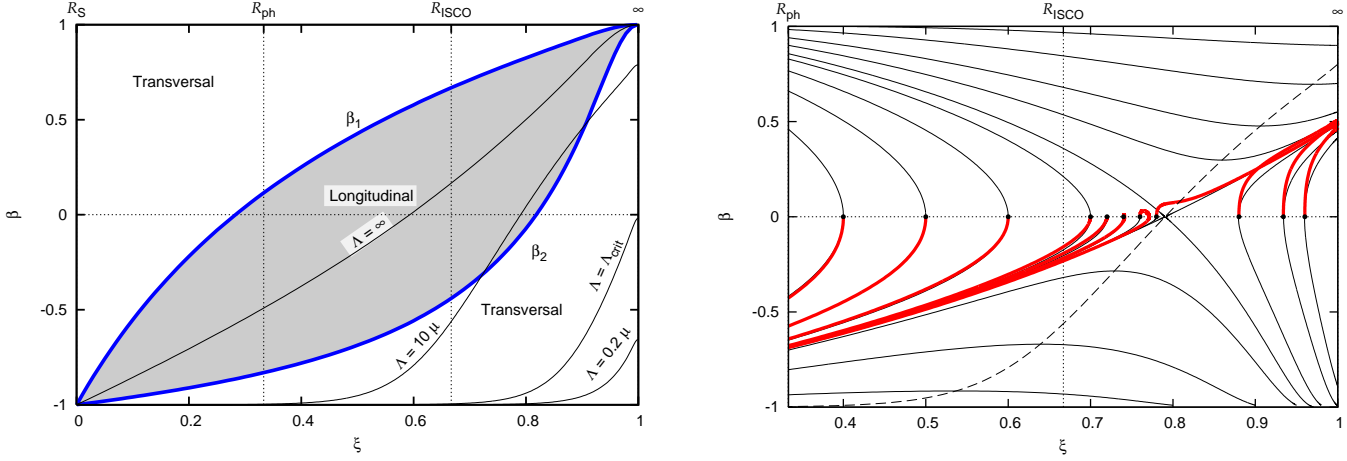
Fig. 3. Left: critical velocities of the cloud motion, $\beta_1(\xi)$ and $\beta_2(\xi)$, at which the observed polarization vector changes its orientation between the longitudinal (inside the shaded region) and the transversal one. The saturation curves $\beta \equiv \beta_0(\xi)$ are also plotted and labelled by the values of the normalized luminosity Λ (for $\Lambda = \Lambda_{\rm crit}$ the saturation velocity vanishes at infinity). Right: several examples of possible trajectories of a warm electron cloud (thick curves). The initial condition is $\beta(t_0) = 0$; the values of $\xi(t_0)$ are indicated by a circle. A monoenergetic distribution of scattering electrons was assumed, $f(\gamma_{\rm e}) = \delta(\gamma_{\rm e} - \langle\gamma_{\rm e}\rangle)$. Cold cloud trajectories are shown for the sake of comparison (thin solid curves). The saturation curve is also plotted (dashed), corresponding to the luminosity parameter $\Lambda = 10\mu$.

$$\bar{P}^{ZZ} = \mathcal{D}^2 \left[P^{xx} \sin^2 \vartheta + \gamma^2 \Delta \left(\cos \vartheta - \beta \right)^2 \right], \tag{12}$$

$$\bar{P}^{YY} = \bar{P}^{yy}, \tag{13}$$

$$\bar{E} = \gamma^2 \left(E - 2\beta F^z + \beta^2 P^{zz} \right), \tag{14}$$

$$\bar{F}^Z = \mathcal{D}\gamma^2 \left(\cos\theta - \beta \right) W. \tag{15}$$

where we denoted $\Delta = \beta^2 E - 2\beta F^z + P^{zz}$ and $W = (1 + \beta^2)F^z - \beta(E + P^{zz})$. Axial symmetry ensures that $\bar{P}^{XY}$ vanishes for the primary radiation field originating from the disk and impinging on the cloud.

Properties of the scattered signal in the static frame of course depend on the motion of the scatterer, which itself results from the interplay of acceleration mechanisms acting on the cloud. In our model the total four-force f^α is a superposition of the radiation and inertial terms. The radiation term is

$$f^\alpha = -\sigma_{\rm T} n_{\rm e} \delta\mathcal{V} \left[\mathcal{C} T^{\alpha\beta} u_\beta - (\mathcal{A} + \mathcal{C}) T^{\rho\sigma} u_\rho u_\sigma u^\alpha \right], \tag{16}$$

where $\delta\mathcal{V}$ is the cloud volume, $\mathcal{C} \equiv 1 + \frac{1}{2}\mathcal{A}$. The change of the cloud internal energy by cooling is

$$\frac{{\rm d}\langle\gamma_{\rm e}\rangle}{{\rm d}s} = -\gamma \mathcal{A} \Lambda \mu \left(E_\star - 2\beta F^z_\star + \beta^2 P^{zz}_\star \right), \tag{17}$$

where we expressed proper time s in units of $R_{\rm S}/c$ and we denote $\mu \equiv m_{\rm p}/m_{\rm e} \simeq 1$ (for electron-proton plasma) or $\mu \simeq 10^3$ (for electron-positron plasma). The parameterisation by μ allows us to consider different types of plasma. However, we note that the radiation field of a standard disk alone is unable to efficiently accelerate protons, and so the case of electron-positron plasma seems to be a more relevant application here (Fukue 2005).

Dynamics of the cloud as a whole is governed by equation of motion in the form

$$\frac{{\rm d}\beta}{{\rm d}s} = \langle\gamma_{\rm e}\rangle^{-1} \mathcal{C}\Lambda\mu \Big[\left(1 + \beta^2\right) F^z_\star$$

$$\left. -\beta \left(E_\star + P^{zz}_\star \right) \right] - \frac{R_{\rm S}}{2\gamma z^2 \xi^{1/2}}, \tag{18}$$

which includes also the black hole gravity. The last two equations couple the cloud trajectory with the evolution of its internal temperature. In order to close the set of equations we need to assume a specific form of the electron energy distribution $f(\gamma_{\rm e})$.

In the case of cold clouds ($\mathcal{A} = 0$, $\mathcal{C} = 1$) the dynamics is characterized by the saturation velocity $\beta_0(\xi)$ to which particles are asymptotically accelerated if inertial effects are small compared to the radiation force (Sikora & Wilson 1981; Icke 1989). This condition corresponds to the limit of $\Lambda \to \infty$, ${\rm d}\beta/{\rm d}s = 0$. We thus obtain

$$\beta(z) \to \beta_0 = \sigma - \sqrt{\sigma^2 - 1}, \quad \sigma \equiv \frac{E_\star + F^z_\star}{2F^z_\star}. \tag{19}$$

Further, for polarization there are two critical velocities, $\beta_1(\xi)$ and $\beta_2(\xi)$, at which the polarization vector changes its orientation between transversal and longitudinal one (this can be seen from the condition $\bar{Q} = 0$). Similar effect of polarization direction changing with velocity of the scattering medium was studied by Beloborodov (1998; for scattering in fast outflows from accretion disks) and Horák & Karas (2005; for radially moving clouds near a compact star). This behaviour is demonstrated in the left panel of figure 3. The right panel shows the corresponding influence of the radiation cooling of the cloud on its bulk motion.

From eq. (18) we find that the motion of warm clouds is governed by the same equation as cold ones, provided that the normalized luminosity is rescaled:

$$\Lambda \to \Lambda' \equiv \langle\gamma_{\rm e}\rangle^{-1} \mathcal{C}\Lambda. \tag{20}$$

In other words, by keeping the disk luminosity at a constant value of the Eddington parameter, the cooling (17)
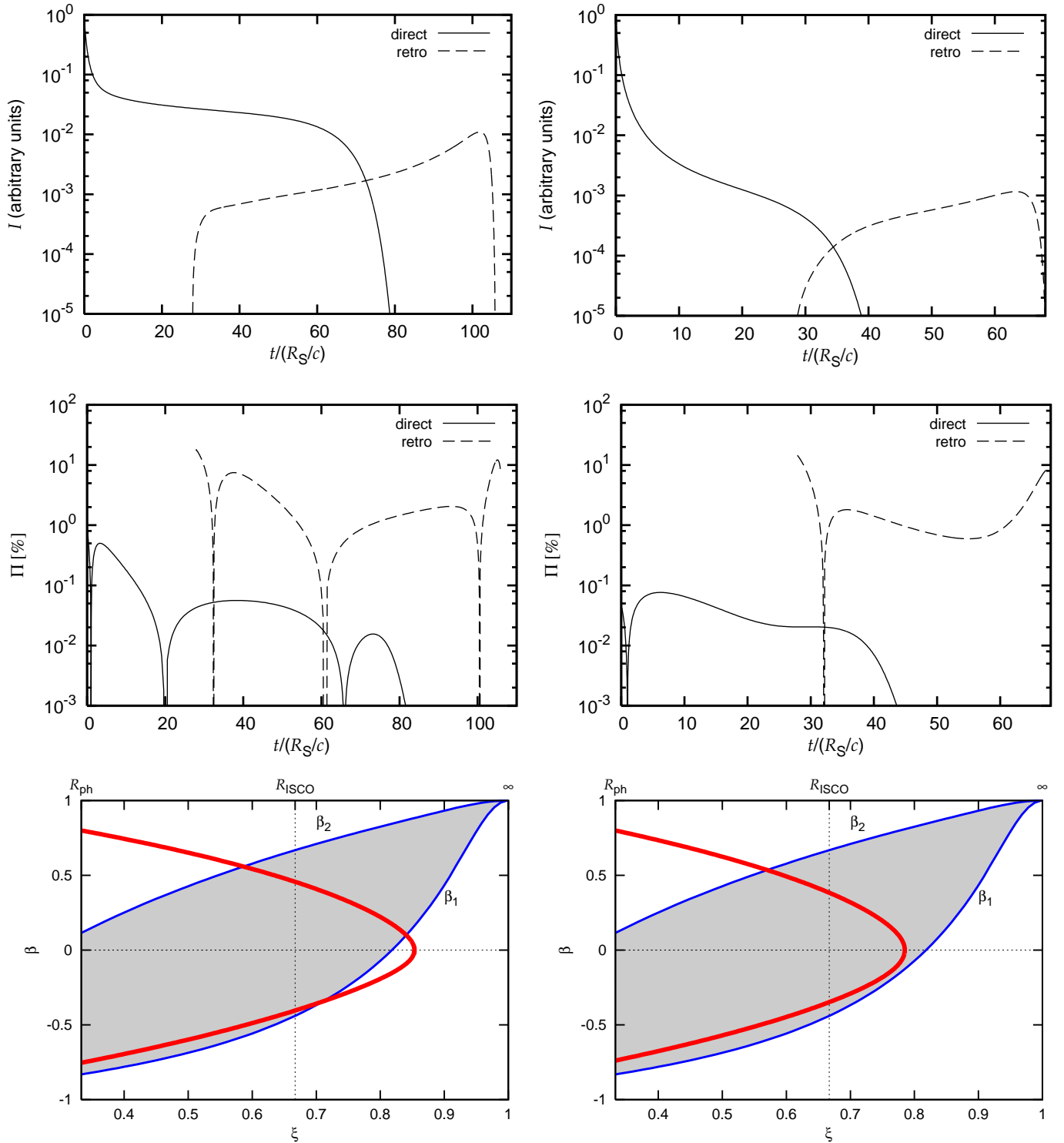
Fig. 4. Comparison between two typical cases with the identical initial conditions except for the cloud temperature: a cold cloud (left panels, $\langle\gamma_e\rangle = 1$) versus a warm cloud (right panels, $\langle\gamma_e\rangle = 3$ at start). Examples are shown of the time behaviour of the observed intensity (top row) and the magnitude of polarization (middle row). Contributions of the retro-lensing images have been summed together and plotted (by a dashed line); they are clearly distinguished from the signal produced by the direct-image photons (solid line). The retro-lensing photons arrive with a certain time delay with respect to the direct photons. The delay is caused by photons taking different path and circling at $r \simeq R_{ph}$ (the effect can be recognized by comparing the relative time shift of the features). We also show, in the bottom row, the corresponding velocity profile $\beta(\xi)$ of the cloud motion. The temperature evolution is given by solving eq. (17) along the trajectory: the warm cloud cools down to $\langle\gamma_e\rangle = 1.3$ along its entire track. Polarization vanishes at the moment when the cloud crosses one of the curves $\beta_1(\xi)$, $\beta_2(\xi)$. In both cases the view angle was $i = 5$ deg, the disk luminosity $\Lambda = 2$. The initial distance $z(t_0) = R_{ph}$ (i.e. $\xi = \frac{1}{3}$), $\beta(t_0) = 0.8$.

gives rise to trajectories gradually deviating from the corresponding cold-cloud limit.

The effect of changing temperature is such that the saturation velocity curve gradually moves across (β, ξ)-plane. This helps us to understand the form of trajectories, which create loops (see fig. 3, right panel). The critical point is given by condition $\beta = 0$, $0 < \xi < \infty$ and it defines the distance where equilibrium between radiation and gravity can be reached. This is a saddle type point, characteristic to an unstable equilibrium, which makes the system behaviour qualitatively different from the case with a central star as a source of primary irradiation (cp. with the critical points examined in Abramowicz et al. 1990). Our result here resembles the case of clouds with non-constant mass, discussed by Keane et al. (2001).

Now we can find the Stokes parameters of scattered light along the cloud path. When determining the temporal evolution of observed intensity and polarization we consider first three images in the observed radiation – the direct (zeroth-order) image and two first-order images. The latter are retro-lensing images formed by rays making a single round about the black hole by the angle $\Phi = 2\pi \pm i$, where i is observer inclination (we denote the retro-lensing images by $\pm$ signs to indicate that they wind up in the opposite directions around the black hole). The higher-order images give a progressively weaker contribution to the final signal, hence we can safely neglect them. The retro-lensing photons give rise to peaks in the observed signal occurring with a characteristic mutual time lag after the direct-image photons. Duration of these features is very short – comparable to the light crossing time – and the time span of the plots can be therefore scaled by $t_{\rm lc} \simeq 1.5 \times 10^{-4} M/(10 M_\odot)$ [sec].

Typical profiles of the resulting lightcurves and polarization curves are shown in figure 4. Here we notice the difference in the lightcurve profiles and the the polarization curves, which is caused by effect of the cloud initial temperature and its gradual cooling. The contribution of the retro-lensing images to the total observed flux is maximum when the scatterer, the black hole and the observer are well-aligned ($i \to 0$) and the scatterer moves towards black hole ($\beta \to -1$). In this situation a non-negligible fraction of photons are scattered toward on the light circular photon orbit, their energy is Doppler boosted, and eventually they are redirected toward the observer. On the other hand, polarization magnitude attains maximum in a slightly different direction whereas, for symmetry reasons, Π vanishes for a strictly aligned observer. The direct image photons are of course most intense in the opposite case ($\beta \to 1$), and so there is an interplay of different orders of the images sensitive to the model parameters.

Identifying the short-duration features in lightcurves could help confirming the existence of the photon circular orbit around the central body, for which black holes are the most likely cause. Polarimetric resolution provides additional information about the source and it could be used to constrain the parameters of the black hole.

4. Discussion and conclusions

In X-rays, future polarimeters could be employed to probe jets and winds in strong gravitational fields of the central compact object. Polarimetry is a powerful tool that can provide additional information, which would be difficult to obtain by other techniques such as traditional photometry and spectroscopy. In this way polarimetry helps to discriminate between different geometries and physical states of sources where accretion processes are accompanied by fast radial motion of the blobs of material. Naturally, this goal would require sufficient sensitivity in X-rays; the scattered signal is mixed with primary photons, which reduce the final polarization. We have seen that the predicted features are flashing for only a brief period of time and the maximum polarization degree is typically $\simeq 1$ percent or less.

In order to allow the analytical treatment we employed various simplifications: we considered the bolometric quantities and the Thomson cross-section for scattering of primary photons on electrons (rather than Compton scattering and the Klein-Nishina cross-section; see Melia & Königl 1989; Skibo et al. 1994; Madau & Thompson 2000). We also assumed that the flow is not magnetically dominated, although astrophysically realistic models require magnetohydrodynamic effects to be taken into account (Begelman et al. 1984; Beskin et al. 2004). Effects of general relativity were taken into account in the limit of the non-rotating black hole spacetime (we neglected the effects of frame-dragging for the sake of simplicity; cf. Vokrouhlický & Karas 1991). Likewise, we adopted the simplest possible parameterization of the disk emissivity via the standard Shakura–Sunyaev model; this could be improved by including relativistic effects (Page & Thorne 1974) and a more realistic description of the disc itself. These changes will be necessary to provide quantitative and astrophysically realistic results for the polarization degree, however, we do not expect any qualitative change regarding the signature of indirect photons. The predicted polarization is either parallel or perpendicular to the projection of cloud velocity onto the observing plane.

References

Abramowicz M. A., Ellis G. F. R., Lanza A., 1990, ApJ, 361, 470
Angel J. R. P., 1969, MNRAS, 158, 219
Begelman M. C., Blandford R. D., Rees M. J., 1984, Rev. Mod. Phys., 56, 255
Begelman M. C., Sikora M., 1987, ApJ, 322, 650

Beloborodov A. M., 1998, ApJ, 496, L105

Beskin V. S., Zakamska N. L., Sol H., 2004, MNRAS, 347, 587

Bonometto S., Cazzola P., Saggion A., 1970, A&A, 7, 292

Chandrasekhar S., 1960, Radiative Transfer (Dover Publ.: New York)

Celotti A., Matt G., 1994, MNRAS, 268, 451

Dolan J. F., 1967, Space Science Reviews, vol. 6, 579

Fukue J., 2005, PASJ, 57, 691

Fukue J., Hachiya M., 1999, PASJ, 51, 185

Fukue J., Tojyo M., Hirai Y., 2001, PASJ, 53, 555

Ghisellini G., Haardt F., Matt G., 2004, A&A, 413, 535

Harris D. E., Krawczynski H., 2002, ApJ, 565, 244

Horák J., 2005, in Proc. of the Workshop on Processes in the Vicinity of Black Holes and Neutron Stars, Vol. 6/7, eds. S. Hledík & Z. Stuchlík (Silesian University, Opava), in press

Horák J., Karas V., 2005, MNRAS, in press (astro-ph/0510532)

Icke V., 1989, A&A, 216, 294

Junor W., Biretta J. A., Livio M., 1999, Nature, 401, 891

Kato S., Fukue J., Mineshige S., 1998, Black-Hole Accretion Disks (Kyoto University Press: Kyoto)

Keane A. J., Barrett R. K., Simmons J. F. L., 2001, MNRAS, 321, 661

Krolik J. H., 1999, Active Galactic Nuclei: From the Central Black Hole to the Galactic Environment (Princeton University Press: Princeton)

Lazzatti D., Rossi E., Ghisellini G., Rees M. J., 2004, MNRAS, 347, L1

Madau P., Thompson C., 2000, ApJ, 534, 239

Melia F., Königl A., 1989, ApJ, 340, 162

Misner C. W., Thorne K. S., Wheeler J. A., 1973, Gravitation (San Francisco: Freeman)

Noerdlinger P. D., 1974, ApJ, 192, 529

O'Dell S. L., 1981, ApJ, 243, L147

Page D. N., Thorne K. S., 1974, ApJ, 191, 499

Phinney E. S., 1982, MNRAS, 198, 1109

Poutanen J., 1994, ApJSS, 92, 607

Renaud N., Henri G., 1998, MNRAS, 300, 1047

Rybicki G. B., Lightman A. P., 1979, Radiative Processes in Astrophysics (Wiley: New York)

Seward F. D., Charles P. A., 1995, Exploring the X-Ray Universe (Cambridge University Press: Cambridge)

Shakura N. I., Sunyaev R. A., 1973, A&A 24, 337

Sikora M., Sol H., Begelman M. C., Madejski M. G., 1996, ApJ, 280, 781

Sikora M., Wilson D. B., 1981, MNRAS, 198, 529

Skibo J. G., Dermer C. D., Kinzer R. L., 1994, ApJ, 426, L23

Tajima Y., Fukue J., 1998, PASJ, 50, 484

Vokrouhlický D., Karas V., 1991, A&A, 252, 835

Watarai K., Fukue J., 1999, PASJ, 51, 725